Nonlinear Dynamics and Systems Theory, **2**(2) (2002) 157–172

Statistical Analysis of Nonimpulsive Orbital Transfers under Thrust Errors, 1

A.D.C. Jesus[1], M.L.O. Souza[2] and A.F.B.A. Prado[2]

[1] *Departamento de Física, Universidade Estadual de Feira de Santana (UEFS), KM. 03 BR. 116 – Campus Universitário, Caixa Postal 252-294, CEP. 44.031-460, Feira de Santana, BA, Brazil*

[2] *Instituto Nacional de Pesquisas Espaciais (INPE), Avenida dos Astronautas 1758, Caixa Postal 515, 12227-010, São Paulo, SP, Brazil*

Received: August 28, 2000; Revised: March 10, 2002

Abstract: In this paper we present the first part of an extensive study of nonimpulsive orbital transfers under thrust errors. We emphasize the first part of the numerical implementation (Monte-Carlo) of the study but mention the first algebraic explanation for some of the numerical results. Its main results suggest and partially characterize the progressive deformation of the trajectory distribution along the propulsive arc, turning 3sigma ellipsoids into banana shaped volumes curved to the center of attraction (we call them "bananoids") due to the loss of optimality of the actual (with errors) trajectories with respect to the nominal (no errors) trajectory.

Keywords: *Orbits; transfer; nonimpulsive; thrust errors; Monte-Carlo analysis.*

Mathematics Subject Classification (2000): 70M20, 65C05, 62L70.

1 Introduction

Most space missions need orbit transfers to reach their goals. These trajectories/orbits are reached sequentially through transfers between them by changing their keplerian elements, by firing apogee motors or other sources of force. These thrusts have linear and/or angular misalignments that displace the vehicle with respect to its nominal directions. The mathematical treatment for these errors can be done by complementary approaches (deterministic, probabilistic, minimax, etc.). In the literature, already reviewed by Souza, *et al.* [1], we highlight.

In the deterministic approach: Rodrigues [2] analyzed the effects of the errors in nonimpulsive thrust on coplanar transfers of a nonpunctual model of a satellite. As such, it is the only work we got considering the attitude motion, the center of mass

misalignments, and the reduction of thrust with use, etc. Santos-Paulo [3] analyzed the effects of errors in impulsive thrusts on coplanar or noncoplanar transfers of punctual model of a satellite. Other related papers are Schultz [4] and Rocco [5].

In the probabilistic approach: Porcelli and Vogel [6] presented an algorithm for the determination of the orbit insertion errors in biimpulsive noncoplanar orbital transfers (perigee and apogee), using the covariance matrices of the sources of errors. Adams and Melton [7] extended such algorithm to ascent transfers under a finite thrust, modeled as a sequence of impulsive burns. They developed an algorithm to compute the propagation of the navigation and direction errors among the nominal trajectory, with finite perigee burns. Rao [8] built a semi-analytic theory to extend covariance analysis to long-term errors on elliptical orbits. Howell and Gordon [9] also applied covariance analysis to the orbit determination errors and they develop a station-keeping strategy of Sun-Earth L1 libration point orbits. Junkins, *et al.* [10] and Junkins [11] discussed the precision of the error covariance matrix method through nonlinear transformations of coordinates. He also found a progressive deformation of the initial ellipsoid of trajectory distribution (due to gaussian initial condition errors), that was not anticipated by the covariance analysis of linearized models with zero mean errors. Its main results also characterize how close or how far are Monte-Carlo analysis and covariance analysis for those examples. Carlton-Wippern [12] proposed differential equations in polar coordinates for the growth of the mean position errors of satellites (due to errors in the initial conditions or in the drag), by using an approximation of Langevin's equation and a first order perturbation theory. Alfriend [13] studied the effects of drag uncertainty via covariance analysis.

In the minimax approach: see russian authors, mainly.

However, all these analyses are approximated. This motivated an exhaustive numerical but exact analysis (by Monte-Carlo), and a partial algebraic analysis done by Jesus [14] under the supervision of the two other authors, to highlight and to study effects not shown in those analyses.

In this work we present the 1^{st} part of the numerical implementation of that Monte-Carlo analysis of the nonimpulsive orbital transfers under thrust vector errors. The results were obtained for two transfers: the first, a low thrust transfer between high coplanar orbits, used by Biggs [15, 16] and Prado [17]; the second, a high thrust transfer between middle noncoplanar orbits (the first transfer of the EUTELSAT II-F2 satellite) implemented by Kuga, *et al.* [18].

The simulations were done for both transfers with minimum fuel consumption. The optimization method used by Biggs [15, 16] and Prado [17] was adapted to the case of transfers with thrust errors. The "pitch" and "yaw" angles were taken as control variables such that the overall minimum fuel consumption defines each burn of the thrusts.

The error sources that we considered were the magnitude errors, the "pitch" and "yaw" direction errors of the thrust vector, as causes of the deviations found in the keplerian elements of the final orbit. Each deviation was introduced separately along the orbital transfer trajectory. We studied two types of errors for each one of these causes: the systematic/constructional/assembly errors (modeled as random-bias) and the operational errors (modeled as white-noise). The random-bias errors are unknown but constants during all the transfer arc, while the white-noise errors change along the transfer arc. These error sources introduced in the orbital transfer dynamics cause effects in the keplerian elements of the final orbit at the final instant.

In this work we present an statistical analysis of the effects of these errors on the mean of the deviations of the keplerian elements of the final orbit with respect to the reference orbit (final orbit without errors in the thrust vector) for both transfers. The

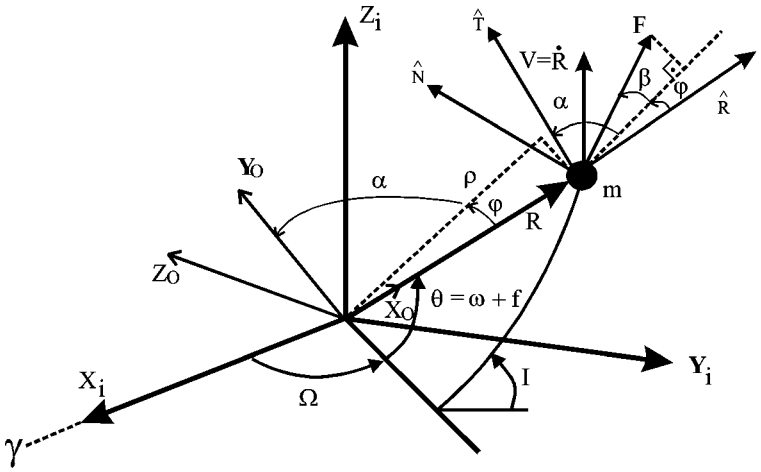

Figure 2.1. Reference system used in this work.

approach that we used in this work for the treatment of the errors was the probabilistic one, assuming these as having zero mean uniform probability density function.

2 Mathematical Formulation and Coordinates Systems

The orbital transfer problem studied can be formulated in the following way:

1) Globally minimize the performance index: $J = m(t_0) - m(t_f)$;
2) With respect to α: $[t_0, t_f] \to R$ ("pitch" angle) and β: $[t_0, t_f]$ ("yaw" angle) with α, $\beta \in C^{-1}$ in $[t_0, t_f]$;
3) Subject to the dynamics in inertial coordinates X_i, Y_i, Z_i of Figure 2.1: $\forall\, t \in [t_0, t_f]$;

$$m\,\frac{d^2X}{dt^2} = -\mu m\,\frac{X}{R^3} + F_x, \tag{1}$$

$$m\,\frac{d^2Y}{dt^2} = -\mu m\,\frac{Y}{R^3} + F_x, \tag{2}$$

$$m\,\frac{d^2Z}{dt^2} = -\mu m\,\frac{Z}{R^3} + F_x, \tag{3}$$

$$\begin{aligned} F_x = F\,[&\cos\beta\sin\alpha\,(\cos\Omega\cos\theta - \sin\Omega\cos I\sin\theta) + \sin\beta\sin\Omega\sin I \\ &- \cos\beta\cos\alpha\,(\cos\Omega\sin\theta + \sin\Omega\cos I\cos\theta)]\,, \end{aligned} \tag{4}$$

$$\begin{aligned} F_y = F\,[&\cos\beta\sin\alpha\,(\sin\Omega\cos\theta + \cos\Omega\cos I\sin\theta) - \sin\beta\cos\Omega\sin I \\ &- \cos\beta\cos\alpha\,(\sin\Omega\sin\theta - \cos\Omega\cos I\cos\theta)] \end{aligned} \tag{5}$$

$$F_z = F\,(\cos\beta\sin\alpha\sin I\sin\theta + \cos\beta\cos\alpha\sin I\cos\theta + \sin\beta\cos I)\,. \tag{6}$$

Or in orbital coordinates (radial R, transversal T, and binormal N) of Figure 2.1:

$$ma_R(t) = F\cos\beta(t)\sin\alpha(t) - \frac{\mu m}{R^2(t)}, \tag{7}$$

$$ma_T(t) = F\cos\beta(t)\cos\alpha(t), \tag{8}$$

$$ma_N(t) = F\sin\beta(t), \tag{9}$$

$$a_R(t) = \dot{V_R} - \frac{V_T^2}{R} - \frac{V_N^2}{R}, \tag{10}$$

$$a_T(t) = \dot{V_T} + \frac{V_R V_T}{R} - V_N \dot{I}\cos\theta - V_N \dot{\Omega}\sin I\sin\theta, \tag{11}$$

$$a_N(t) = \dot{V_N} + \frac{V_R V_N}{R} + V_T \dot{I}\cos\theta + V_T \dot{\Omega}\sin I\sin\theta, \tag{12}$$

$$V_R = \dot{R}, \tag{13}$$

$$V_T = R(\dot{\Omega}\cos I + \dot{\theta}), \tag{14}$$

$$V_N = R(-\dot{\Omega}\sin I\cos\Omega + \dot{I}\sin\Omega), \tag{15}$$

$$\theta = \omega + f. \tag{16}$$

These equations were obtained by: 1) writing in coordinates of the dexterous rectangular reference system with inertial directions $OX_iY_iZ_i$ the Newton's laws for the motion of a satellite with mass m, with respect to this reference system, centered in the Earth's center of mass O with X_i axis toward the Vernal point, X_iY_i plane coincident with Earth's Equator, and Z_i axis toward the Polar Star approximately; 2) rewriting them in coordinates of the dexterous rectangular reference system with radial, transversal, binormal directions SRTN, centered in the satellite center of mass; helped by 3) a parallel system with $OX_oY_oZ_o$ directions, centered in the Earth's center of mass O, X_o axis toward the satellite, X_oY_o plane coincident with the plane established by the position R and velocity V vectors of the satellite, and Z_o axis perpendicular to this plane; and helped by 4) the instantaneous keplerian coordinates (Ω, I, ω, f, a, e). These equations were later rewritten and simulated by using 5) 9 state variables, defined and used by Biggs [15, 16] and Prado [17], as functions of an independent variable s shown in Figure 2.2.

The nonideal thrust vector, with magnitude and direction errors, is given by:

$$\vec{F_E} = \vec{F} + \Delta\vec{F}, \tag{17}$$

$$\vec{F_E} = \vec{F_R} + \vec{F_T} + \vec{F_N}, \tag{18}$$

$$|\vec{F_E}| = F_E, \qquad |\vec{F}| = F, \tag{19}$$

$$F_R = (F + \Delta F)\cos(\beta + \Delta\beta)\sin(\alpha + \Delta\alpha), \tag{20}$$

$$F_T = (F + \Delta F)\cos(\beta + \Delta\beta)\cos(\alpha + \Delta\alpha), \tag{21}$$

$$F_N = (F + \Delta F)\sin(\beta + \Delta\beta), \tag{22}$$

where: $\vec{F}$, $\vec{F_E}$ and $\Delta\vec{F}$ are: the thrust vector without errors, the thrust vector with errors, and the error in the thrust vector, respectively; $\Delta\alpha$ e $\Delta\beta$ are the errors in the

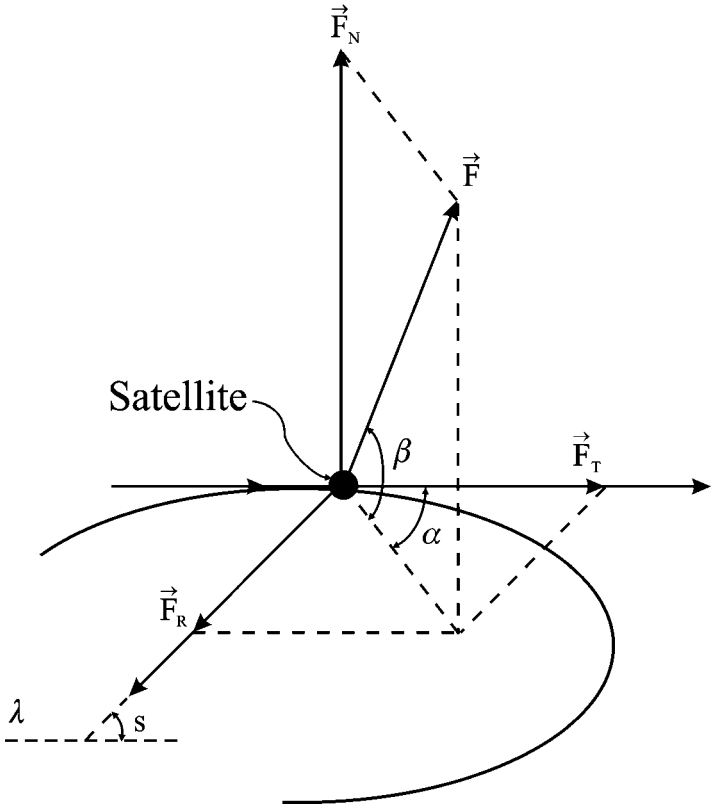

Figure 2.2. Thrust vector applied to the satellite and the s variable.

"pitch" and in the "yaw" angles, respectively; F_R, F_T e F_N are the components of the thrust vector with errors $\vec{F_E}$ in the radial, transversal and normal directions, respectively. The magnitude error, ΔF, was computed as a percentage of the nominal force, while the direction errors $\Delta\alpha$ and $\Delta\beta$ were computed in units of angle. They are varied inside given ranges, that is, $\pm DES1.F$ for ΔF, $\pm DES2$ for $\Delta\alpha$ and $\pm DES3$ for $\Delta\beta$. This variation will correspond to the implementation of the random numbers that satisfy a uniform probability distribution into those ranges. In this way, for each implementation of the orbital transfer arc, values of α and β are chosen, whose errors are inside the range, that produce the direction for the overall minimum fuel consumption.

3 Numerical Results

The simulations were performed with 1000 realizations for each transfer, that is, 1000 runs were done with random values for each DES1, DES2 and DES3, such that the results obtained for the final keplerian elements represent the arithmetic mean of 1000 realizations (mean over the ensemble). The value 1000 was chosen to represent the set of runs because the mean deviations in all final keplerian elements with respect to their references converge to their minimal for this number of runs.

Figures 3.1 and 3.2 show the mean deviations in the final semi-major axis and eccentricity versus the number of runs, respectively. These plots were done for systematic pitch direction with $DES2 = 1,0^o$.

The computation of the mean deviations of the final keplerian elements with respect to their references can be estimated by the arithmetic mean of them, for 1000 runs as representatives. So, we can estimate mean deviation of any final keplerian element, ΔK as

$$\overline{\Delta K} = E\{\Delta K\} = \int_{-\infty}^{\infty} \xi f_{\Delta K}(\xi)\, d\xi \cong \sum_{i=1}^{N=1000} \frac{\Delta K_i}{N}. \tag{23}$$

It is important to remark that equation (23) estimates a mean in the ensemble and not in the time. In this work we present only these estimates for the final semi-major axis and eccentricity with respect to their reference. Figures 3.3 to 3.14 present the behavior of them as functions of the maximum (random-bias and white noise) direction errors. For the random-bias errors we found the following results:

1) Uniform random-bias errors: semi-major axis(a), "pitch" errors.

We observe, in these plots (Figure 3.3 and Figure 3.4), behaviors very similar for both maneuvers, although they are very different from each other. We easily observe that the values of the mean semi-major axis present a region of decrease sufficiently defined according to the growth of the maximum "pith" error, DES2. These figures suggest a nonlinear law between these elements for both cases, that is, they suggest a cause vs. effect relation in the orbital transfer phenomenon, not depending of the maneuver studied.

2) Uniform random-bias errors: semi-major axis(a), "yaw" errors

Once more these plots (Figure 3.5 and Figure 3.6) show behaviors well defined and similar for the semi-major axis as function of the maximum "yaw" error, DES3, for both maneuvers studied. That is, there is a region of decrease well defined between the elements a and DES3.

3) Uniform random-bias errors: eccentricity(e), "pitch" and "yaw" errors.

These plots show (Figure 3.7 and Figure 3.8) the nonlinear behavior of the mean final eccentricity with the maximum "pitch" and "yaw" deviations. They were done only for the second maneuver because in the first one the change of the eccentricity is close to zero for the usual values of DES2 and DES3. They were plotted with precision of 10^{-3} for the eccentricity.

For the white-noise errors the results were very similar to the results obtained for the random-bias errors but, the curves for the "pitch" errors present a more defined pattern with respect to those for the "yaw" errors, where small fluctuations appear in its final form. It is possible to see that the influence of the out-of-plane ("yaw") errors is so strong in the definition of the orbital transfer trajectory.

4) Uniform white-noise errors: semi-major axis(a), "pitch" errors.

The Figures 3.9 and 3.10 show the results for white-noise "pitch" errors in the semi-major axis.

5) Uniform white-noise errors: semi-major axis(a), "yaw" errors.

The Figures 3.11 and 3.12 show the results for white-noise "yaw" errors in the semi-major axis.

Figures 3.9 to 3.12 show clearly the influence of the white-noise errors when the second maneuver is simulated with errors in "yaw". The region of decrease still exist, as well as

the nonlinear relation, but there are fluctuations in the growth of the maximum "yaw" error.

6) Uniform white-noise errors: eccentricity(e), "pitch" and "yaw" errors.

These plots (Figures 3.13 and 3.14) show that the values of the eccentricity also fluctuate for practical maneuvers with the white-noise errors in "yaw", but keeping the region of growth similar to the one verified for the random-bias errors case. So, we can say that all these results suggest and partially characterize the progressive deformation of the trajectory distribution along the propulsive arc. It occurs due to the loss of optimality of the actual trajectories (with errors) with respect to the nominal trajectories (without errors).

The dependence of the final keplerian elements with the magnitude errors for any of the cases was practically null, specially for the mean deviation of the final semi-major axis, since the perturbations occurred in this element were probably due to its estimator and they were comparable to the numerical errors of the experiment, as shown in Figures 3.15 and 3.16. They show that the mean deviation in the final semi-major axis is much smaller than the cone $\pm 1\sigma$(standard deviation of the deviation in the final semi-major axis).

The values for DES1, DES2 and DES3 used in these plots range from usual values to nonusual values, with the aim to verify the general behaviors. Obviously, it is not usual to have a "pitch" error equal to $30,0^o$ or a magnitude error equal to $30,0\%$, for example.

Conclusions

This work presented results of the thrust vector errors implementation for nonimpulsive orbital transfer maneuvers. It was verified that, in any case, the mean deviation in the final semi-major axis presents a nonlinear (approximately parabolic) dependence with the maximum error in thrust direction. The same results were verified for the mean deviation in the final eccentricity, for the second transfer. The respective dependencies with the thrust magnitude errors were not verified. The general results suggest a progressive deformation of the trajectory distribution along the propulsive arc. This deformation may be associated to the loss of the optimality of the actual trajectories with respect to the nominal trajectory.

Acknowledgments

The partial financial support from CAPES (Brazilian agencie) is acknowledged.

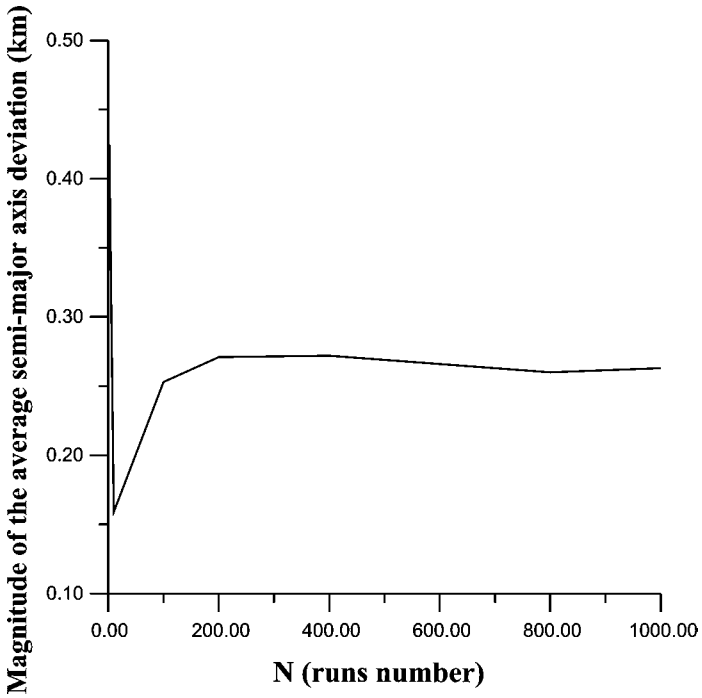

Figure 3.1. Magnitude of the average semi-major axis deviations vs. N.

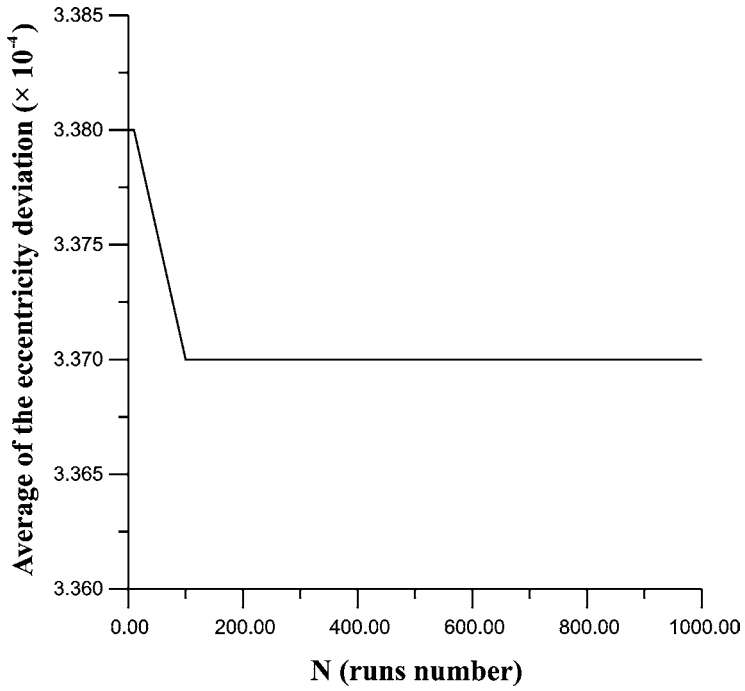

Figure 3.2. Average of the eccentricity $(\times 10^{-4})$ deviation vs. N.

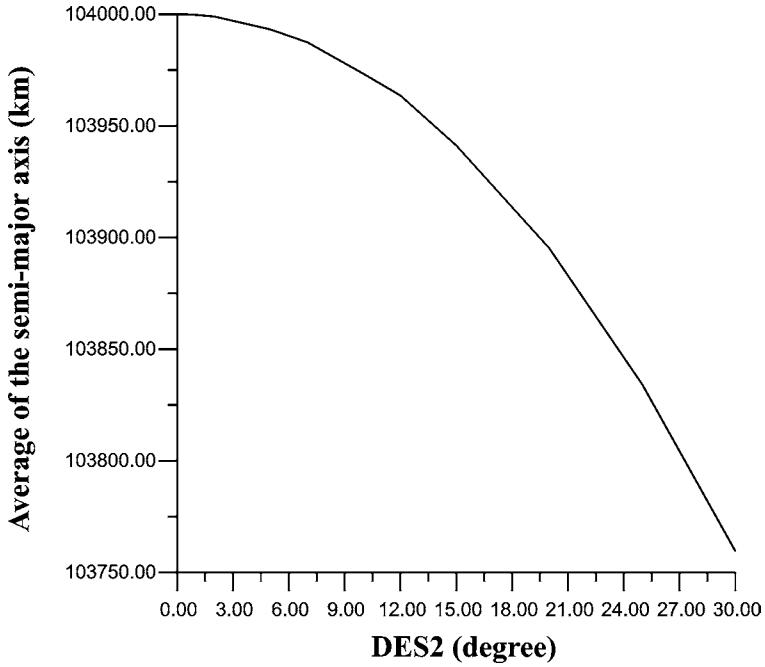

Figure 3.3. First Maneuver: $E\{a(t_f)\}$ vs. $DES2$.

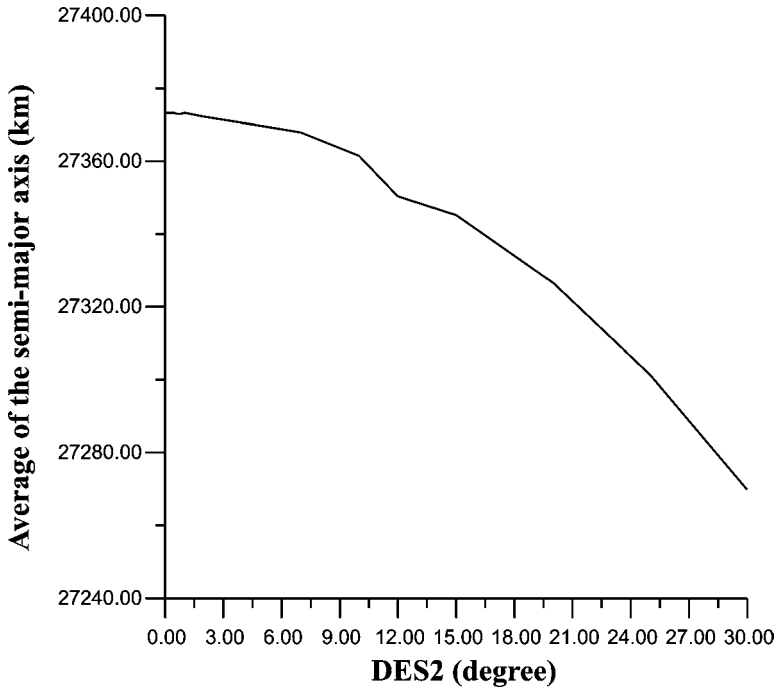

Figure 3.4. Second Maneuver: $E\{a(t_f)\}$ vs. $DES2$.

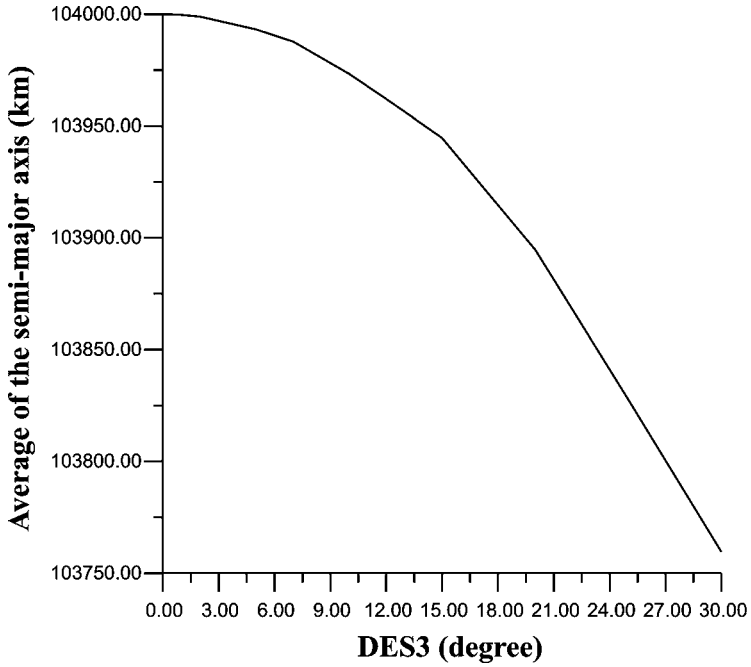

Figure 3.5. First Maneuver: $E\{a(t_f)\}$ vs. $DES3$.

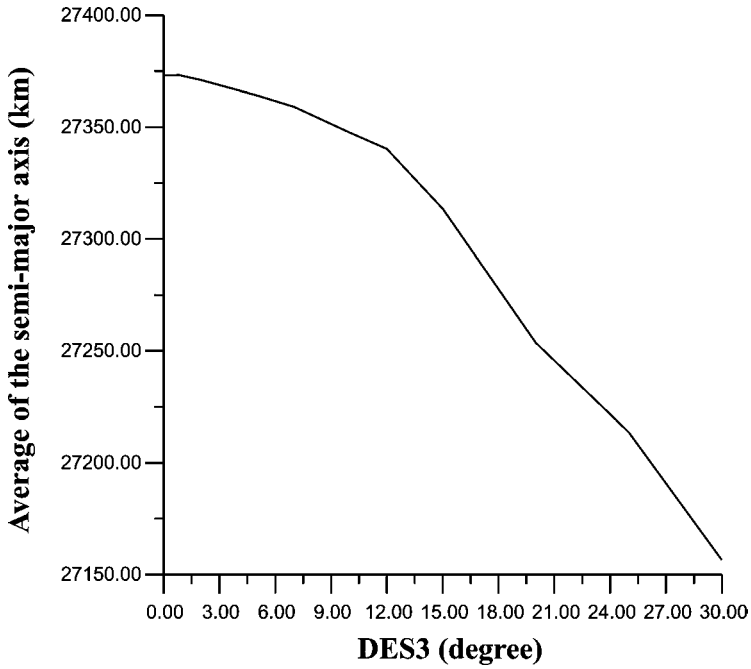

Figure 3.6. Second Maneuver: $E\{a(t_f)\}$ vs. $DES3$.

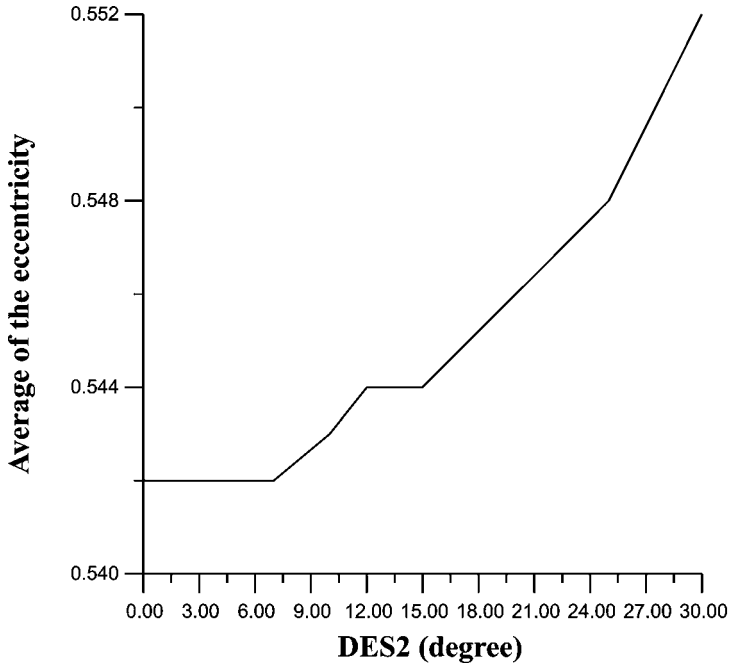

Figure 3.7. Second Maneuver: $E\{e(t_f)\}$ vs. $DES2$.

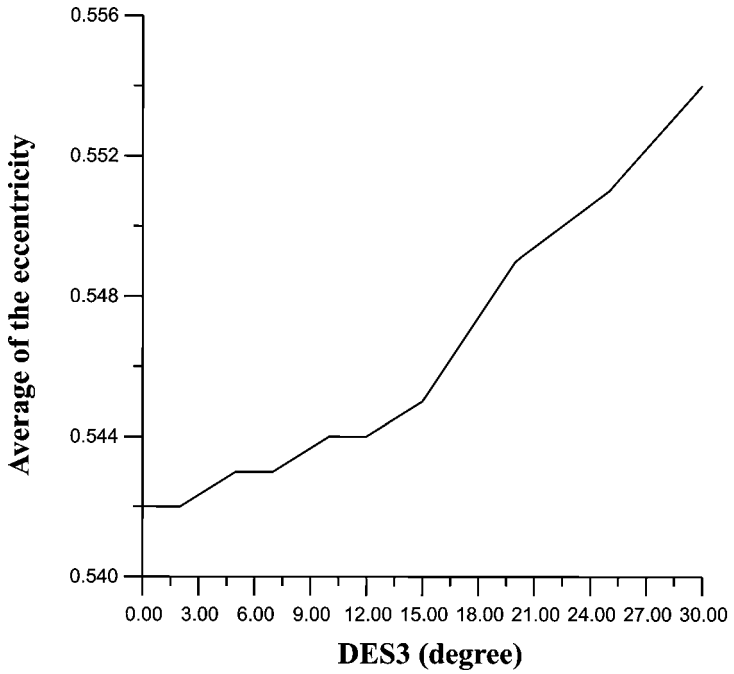

Figure 3.8. Second Maneuver: $E\{e(t_f)\}$ vs. $DES3$.

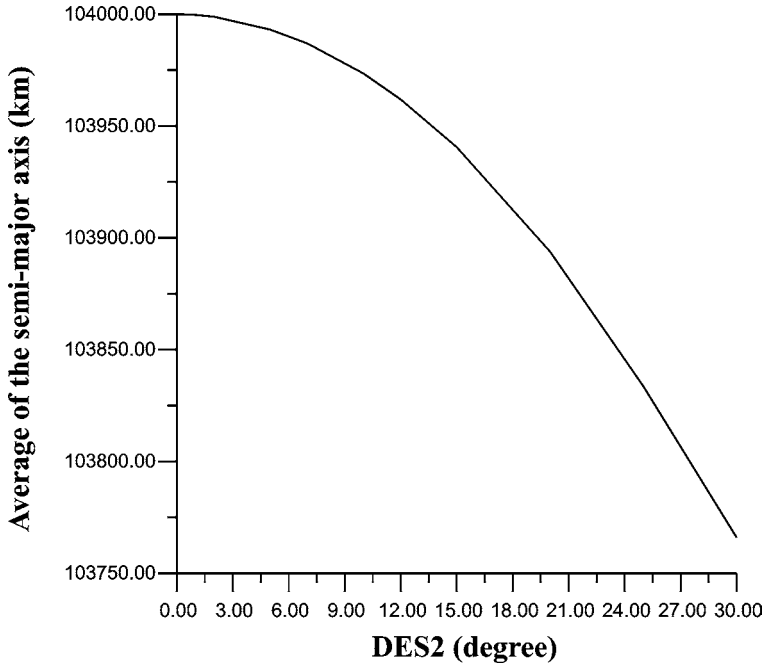

Figure 3.9. First Maneuver: $E\{a(t_f)\}$ vs. $DES2$.

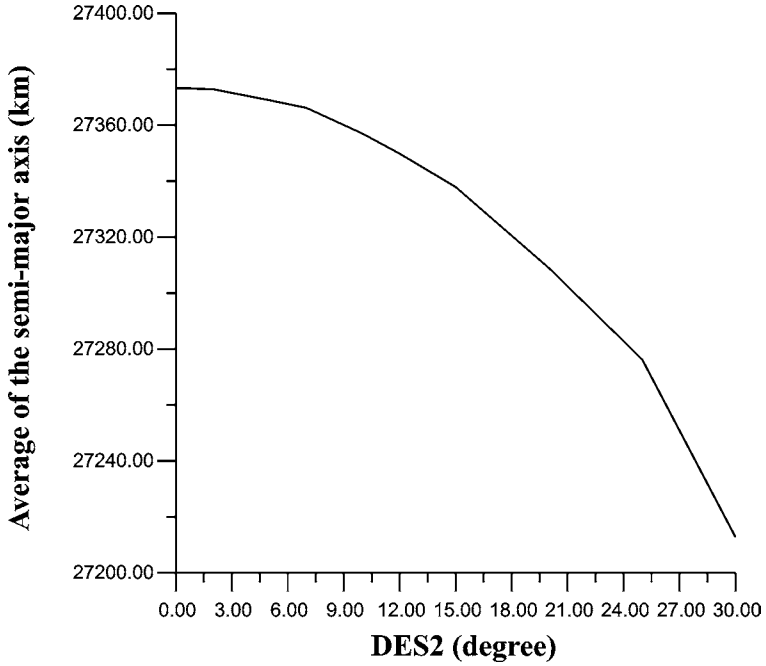

Figure 3.10. Second Maneuver: $E\{a(t_f)\}$ vs. $DES2$.

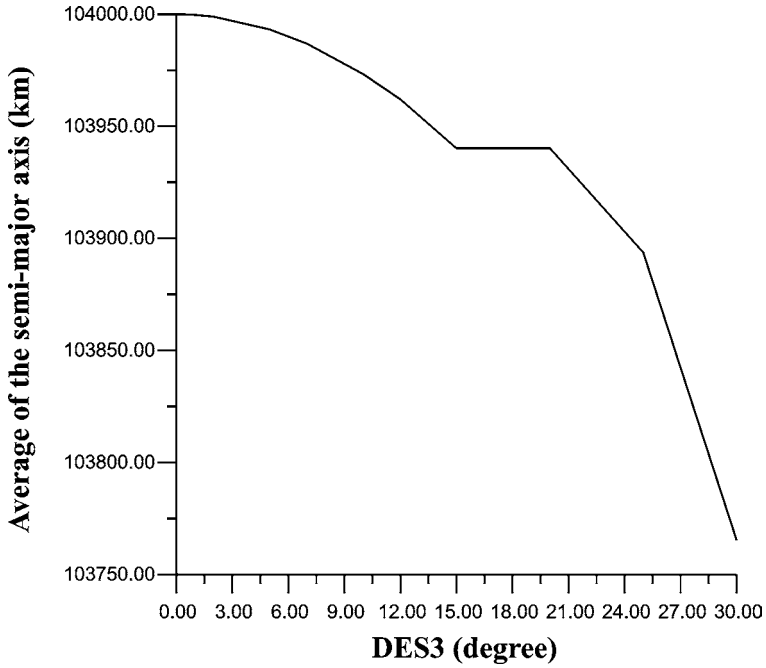

Figure 3.11. First Maneuver: $E\{a(t_f)\}$ vs. $DES3$.

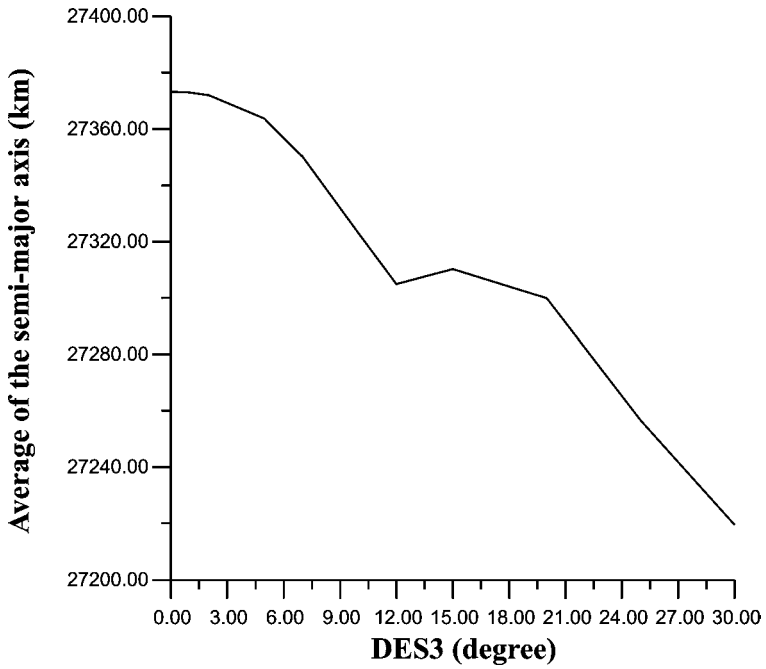

Figure 3.12. Second Maneuver: $E\{a(t_f)\}$ vs. $DES3$.

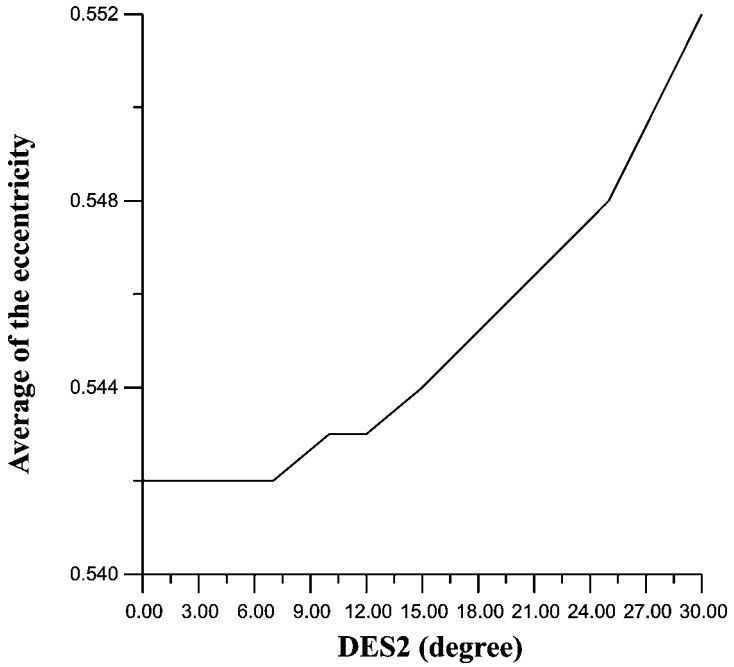

Figure 3.13. Second Maneuver: $E\{e(t_f)\}$ vs. $DES2$.

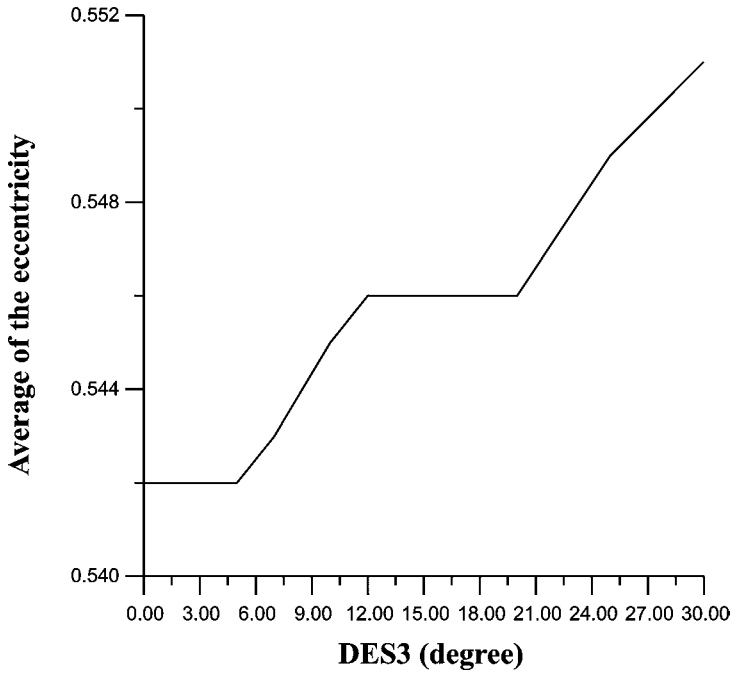

Figure 3.14. Second Maneuver: $E\{e(t_f)\}$ vs. $DES3$.

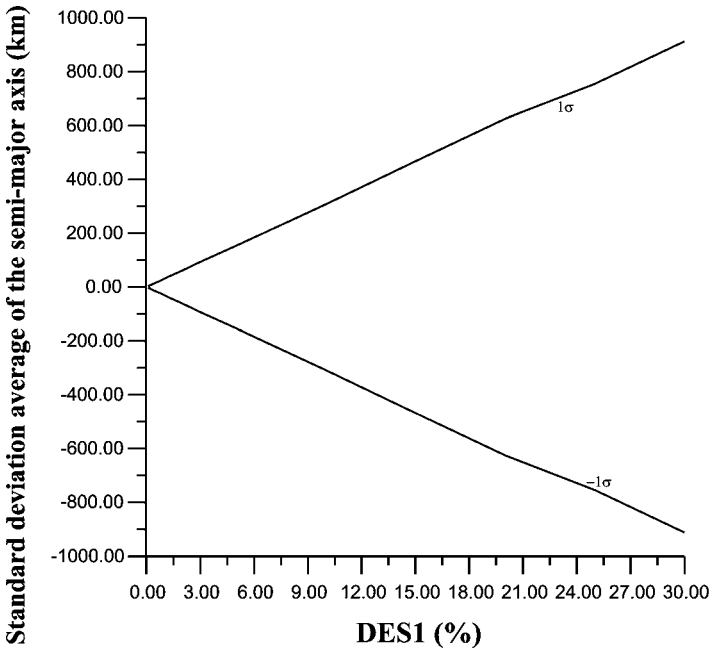

Figure 3.15. First Maneuver: $E\{\Delta a(t_f)\}$ vs. $DES1$ and its σ (standard deviation).

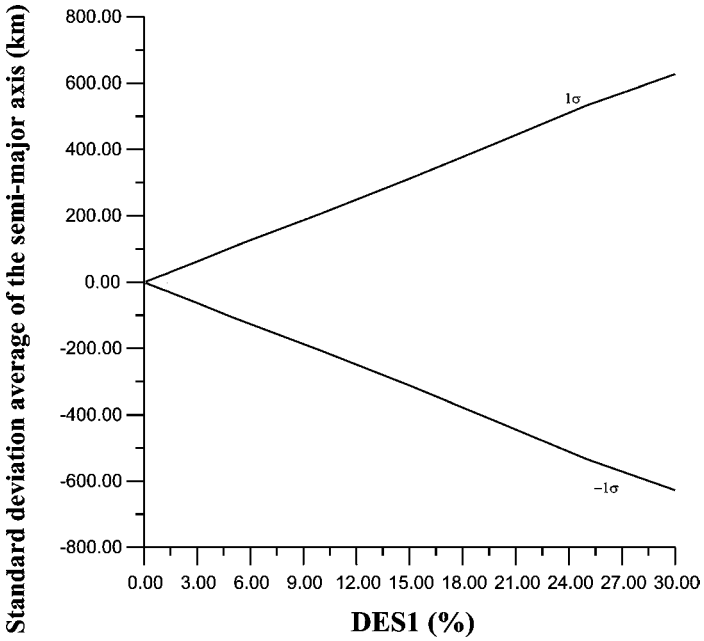

Figure 3.16. Second Maneuver: $E\{\Delta a(t_f)\}$ vs. $DES1$ and its σ (standard deviation).

References

[1] Souza, M.L.O., Prado, A.F.B.A., Rodrigues, D.L.F., Santos-Paulo, M.M.N., Jesus, A.D.C. and Rocco, E.M. A discussion on the effects of thrust misalignments on orbit transfers. *Proceedings of the XXI Congresso Nacional de Matemtica Aplicada e Computacional*, Caxambu, MG, Brasil, September 14-18, 1998, pp. 73–89.

[2] Rodrigues, D.L.F. Análise dinâmica da transferência orbital. Master Dissertation. Instituto Nacional de Pesquisas Espaciais (INPE), São José dos Campos, São Paulo, Brasil, 1991.

[3] Santos-Paulo, M.M.N. Estudo da influência dos erros dos propulsores em manobras orbitais tridimensionais. Master Dissertation. Instituto Nacional de Pesquisas Espaciais (INPE). São José dos Campos, São Paulo, Brasil, 1998.

[4] Schultz, W. Transferências biimpulsivas entre órbitas elípticas não coplanares com consumo mínimo de combustível. Master Dissertation. Instituto Nacional de Pesquisas Espaciais (INPE), São José dos Campos, São Paulo, Brasil, 1997.

[5] Rocco, E.M. Manutenção orbital de constelações de satélites simétricas com manobras impulsivas ótimas com limite de tempo. Doctoral Thesis (on going). Instituto Nacional de Pesquisas Espaciais (INPE), São José dos Campos, São Paulo, Brasil, 1999.

[6] Porcelli, G. and Vogel, E. Two-impulse orbit transfer error analysis via covariance matrix. *Journal of Spacecraft and Rockets* **17**(3) (1980) 285–255.

[7] Adams, N.J. and Melton, R.G. Orbit transfer error analysis for multiple, finite perigee burn, ascent trajectories. *The Journal of Astronautical Sciences* **34**(4) (1986) 355–373.

[8] Rao, K.R. Orbit error estimation in the presence of force model errors. *AAS Paper 93-254, Advances in the Astronautical Sciences* **84**(1) (1993) 61–74.

[9] Howell, K.C. and Gordon, S.C. Orbit determination error analysis and a station-keeping strategy for Sun-5-Earth L1 libration point orbits. *The Journal of Astronautical Sciences* **42**(2) (1994) 207–228.

[10] Junkins, J.L., Akella, M.R. and Alfried, K.T. Non-gaussian error propagation in orbit mechanics. *The Journal of the Astronautical Sciences* **4**(4) (1996) 541–563.

[11] Junkins, J.L. Adventures on the interface of dynamics and control. *Journal of Guidance, Control, and Dynamics* **20**(6) (1997) 1058–1071.

[12] Carlton-Wippern, K.C. Satellite position dilution of precision (SPDOP). *AAS/AIAA Astrodynamics Specialist Conference*, Sun Valley, Idaho, EUA, August 4-7, 1997, (AAS 97-609).

[13] Alfriend, K.T. Orbit uncertainty due to drag uncertainty. 14^{th} *International Symposium on Spaceflight Systems and Data Control*, Iguassu Falls, Parana, Brazil, February 8-12, 1999.

[14] Jesus, A.D.C. Análise estatística de manobras orbitais com propulsão finita sujeita a erros no vetor empuxo. Doctoral Thesis. Instituto Nacional de Pesquisas Espaciais (INPE), São José dos Campos, São Paulo, Brasil, 1999.

[15] Biggs, M.C.B. The Optimisation of Spacecraft Orbital Manoeuvres. Part I: Linearly Varying Thrust Angles. Connecticut, USA: The Hatfield Polytechnic, Numerical Optimisation Centre, 1978. 24p. (The Hatfield Polytechnic – Technical Report 98).

[16] Biggs, M.C.B. The optimisation of spacecraft orbital manoeuvres. Part II: Using Pontryagin's Maximum Principle. Connecticut, USA: The Hatfield Polytechnic, Numerical Optimisation Centre, 1979. 27p. (The Hatfield Polytechnic – Technical Report 101).

[17] Prado, A.F.B.A. Análise, seleção e implementação de procedimentos que visem manobras ótimas de satélites artificiais. Master Dissertation. Instituto Nacional de Pesquisas Espaciais (INPE), São José dos Campos, São Paulo, Brasil, 1989.

[18] Kuga, H.K., Gill, E. and Montenbruck, O. Orbit determination and apogee boost maneuver estimation using UD filtering. Wessling: DLR-GSOC, 1991. (Internal report DLR-GSOC IB 91-2).